

G2 histone methylation is required for the proper segregation of chromosomes

Ryan Heit¹, Jerome B. Rattner², Gordon K. T. Chan¹ and Michael J. Hendzel^{1,*}

¹Department of Oncology, Faculty of Medicine, University of Alberta, Edmonton, Canada T6G 1Z2

²Departments of Cell Biology and Anatomy, Biochemistry and Molecular Biology, and Oncology, Faculty of Medicine, University of Calgary, Calgary, Canada T2N 4N1

*Author for correspondence (michaelh@cancerboard.ab.ca)

Accepted 18 May 2009

Journal of Cell Science 122, 2957-2968 Published by The Company of Biologists 2009
doi:10.1242/jcs.045351

Summary

Trimethylation of lysine 9 on histone H3 (H3K9me3) is known both to be necessary for proper chromosome segregation and to increase in late G2. We investigated the role of late G2 methylation, specifically in mitotic progression, by inhibiting methylation for 2 hours prior to mitosis using the general methylation inhibitor adenine dialdehyde (AdOx). AdOx inhibits all methylation events within the cell but, by shortening the treatment length to 2 hours and studying mitotic cells, the only methylation events that are affected are those that occur in late G2. We discovered that methylation events in this time period are crucial for proper mitosis. Mis-segregation of chromosomes is observed with AdOx treatment. Through studies of histone modifications, we have found that inhibiting late G2 methylation affects trimethylation of H3K9 and H4K20. The mitotic checkpoint is active and many kinetochore proteins localize properly, however, pericentric chromatin in these cells is found to be less compact (dense). The reduced integrity of

pericentric heterochromatin might be responsible for a noted loss of tension at the centromere in AdOx-treated cells and activation of the spindle assembly checkpoint. We postulate that late G2 methylation is necessary for proper pericentric heterochromatin formation. The results suggest that a reduction in heterochromatin integrity might interfere both with microtubule attachment to chromosomes and with the proper sensing of tension from correct microtubule-kinetochore connections, either of which will result in activation of the mitotic checkpoint.

Supplementary material available online at
<http://jcs.biologists.org/cgi/content/full/122/16/2957/DC1>

Key words: Chromosome alignment, Methylation, Mitotic checkpoint, Pericentric heterochromatin, SUV39

Introduction

We have previously demonstrated that trimethylation on lysine 9 of histone H3 (H3K9me3) dramatically increases in G2 to reach a maximum at metaphase and then rapidly declines during entry into the next interphase (McManus et al., 2006). The loss of lysine 9 trimethylation in mouse embryonic fibroblast cells double-null for histone-lysine-N-methyl transferase (*SUV39h1/h2*^{-/-} cells) correlates with mitotic defects such as chromosomes that fail to align, which can result in aneuploidy (McManus et al., 2006; Peters et al., 2001). This methylation cycle is independent of histone replacement and, thus, appears to involve a methylation-demethylation cycle (McManus et al., 2006). The trimethylation of H3K9 is catalyzed by SUV39h1 and SUV39h2, both of which are believed to catalyze the trimethylation of lysine 9 specifically (Rea et al., 2000).

With the recent identification of histone lysine demethylases, we now know that methyl groups turnover on histones. To date, lysine demethylases include several Jumonji domain containing proteins as well as an amine oxidase, LSD1 (Agger et al., 2007; Cloos et al., 2006; De Santa et al., 2007; Fodor et al., 2006; Hong et al., 2007; Klose et al., 2006; Shi et al., 2004; Tsukada et al., 2006; Xiang et al., 2007). These demethylases are specific to certain methylated lysines. For example, LSD1 demethylates mono- and dimethyl forms of lysine 4 on histone H3 (H3K4me1 and H3K4me2, respectively) (Shi et al., 2004) and JMJD3 (Jumonji domain containing 3) seems to be specific for H3K27 (Agger et al., 2007; De Santa et al., 2007; Hong et al., 2007; Xiang et al., 2007). These newly characterized demethylases help to explain the cell-cycle-dependent changes in

H3K9me3 abundance, and also imply the existence of a dynamic equilibrium between methylation and demethylation events. The extent of methylation dynamics, however, must be low because studies examining the turnover of radiolabel on histone proteins revealed that the lifetime of the methylation paralleled the lifetime of the histone and was greater than the time required to complete a cell cycle (Annunziato et al., 1995; Borun et al., 1972). Thus, dynamic methylation must be either restricted to brief periods of the cell cycle, such that a pulse-label experiment might not sufficiently represent this period of time, or it must be restricted to a small subset of methylated lysines (either site-specific or reflecting the dynamics of specific small pools of histones).

To date, the established roles of histone methylation, such as the regulation of gene expression (Rea et al., 2000), X-inactivation (Rougeulle et al., 2003) and cell differentiation (Kubicek et al., 2006), suggest stability in the methylated forms of histones. These roles require a methylation mark that is stable over successive cell cycles. The more recent findings involving a dynamic methylation equilibrium described above imply that methylation might have an additional role that acts on a much shorter time scale. Specifically, the findings that H3K9 methylation is cell cycle-dependent (McManus et al., 2006) and findings that suggest that H3K9me3 must be very tightly regulated [both the over-expression (Melcher et al., 2000) and the loss (Peters et al., 2001) of SUV39h1 results in mitotic defects] lead us to hypothesize that late G2 methylation is important for mitotic progression and chromosome segregation.

The H3K9me3 modification is required for the formation and maintenance of heterochromatin (Gonzalo et al., 2005; Schotta et al., 2004; Zinner et al., 2006). This maintenance involves a cyclical pathway involving many proteins. Histone amino-terminal acetylation interferes with heterochromatin structure and its removal by histone deacetylase (HDAC) complexes is required prior to H3K9 methylation (Xin et al., 2004). DNA methylation, accomplished by DNA methyltransferases (DNMT), is also required for H3K9 methylation (Xin et al., 2004). Once established, the H3K9me3 modification recruits heterochromatin protein 1 (HP1) (Bannister et al., 2001; Fischle et al., 2005; Lachner et al., 2001; Nakayama et al., 2001), which allows the binding of numerous proteins needed for heterochromatin formation, among them DNMT1 and HDACs (Lechner et al., 2005; Smallwood et al., 2007; Smothers and Henikoff, 2000; Yamada et al., 2005; Zhang et al., 2002) (for a review, see Grewal and Jia, 2007). The heterochromatin formation pathway is needed for mitosis because the loss of HDACs has been shown to disrupt pericentric heterochromatin and inhibit proper chromosome segregation (Cimini et al., 2003; Robbins et al., 2005; Stevens et al., 2008). The experimental protocols of the previous studies involved time periods of several cell cycles. By contrast, our earlier study indicates that maintenance of heterochromatin might be dependent on active late G2 methylation, meaning that it is required in every cell cycle.

To test the importance of late G2 methylation in chromosome segregation, we inhibited protein methylation for brief periods using the general methylation inhibitor adenosine dialdehyde (AdOx) (Bartel and Borchardt, 1984). We found that inhibiting methylation solely in late G2 leads to mitotic defects. We also observed that several methylated histones (H3K9me3, H4K20me3 and H4K20me1) are significantly affected by this exposure to AdOx in G2. Further, we observed centromeric and kinetochore structural defects and chromosome misalignment in AdOx-treated mitotic cells. By indirect immunofluorescence (IIF), we show that specific kinetochore proteins are affected by the loss of active methylation. Although the mitotic checkpoint was found to be intact and properly activated, the checkpoint eventually fails after several hours of mitotic arrest, resulting in either aneuploidy, tetraploidy or cell death. These results indicate that methylation events during late G2 might operate to maintain and ensure the density and structural integrity of pericentric heterochromatin prior to mitosis. The results suggest that intact dense pericentric heterochromatin is required for the proper sensing of kinetochore tension and for inactivation of the mitotic checkpoint.

Results

Mitotic defects found in HeLa cells treated with AdOx

In order to test whether or not protein methylation events that occur during entry into mitosis, such as the trimethylation of histone H3 lysine 9, are functionally important, we examined the effects of AdOx on asynchronous HeLa cell cultures by IIF. AdOx is known to be a general methylation inhibitor that inhibits *S*-adenosylhomocysteine hydrolase (Keller and Borchardt, 1987). This leads to inhibition of *S*-adenosylmethionine-dependent methylation events in the cell (Bartel and Borchardt, 1984). If a protein methylation event, such as the G2 trimethylation of lysine 9, were crucial for proper chromosome alignment, we would expect that short treatments with AdOx would lead to mitotic defects. To test this, cells were treated with 250 μ M AdOx for 2 hours and then analyzed. This resulted in a prominent cell defect in mitosis, but non-mitotic cell viability was unaffected. Fig. 1 shows representative cells with mitotic defects after AdOx treatment. The defect is

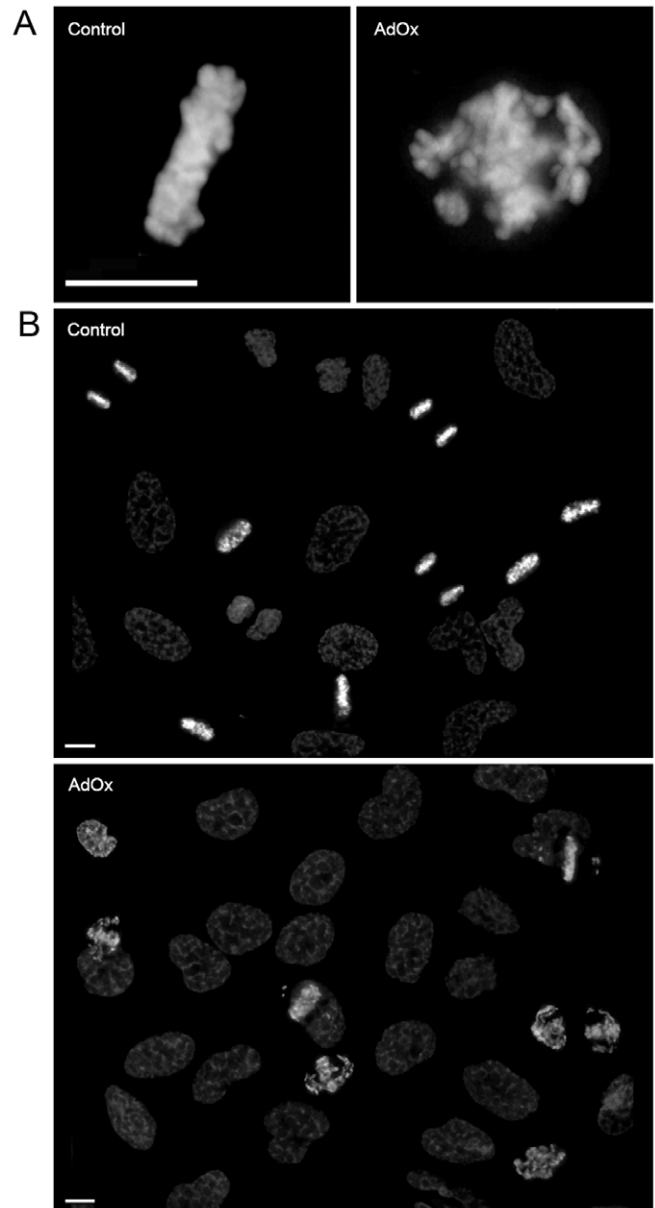


Fig. 1. High-resolution images of DNA stain in mitotic HeLa cells.

(A) Representative digital images of metaphase HeLa cells immunofluorescently labeled with the DNA binding dye, DAPI. A representative high-resolution image of a cell treated for 2 hours with AdOx (right image) is compared to a control (left image). Depicted in the AdOx-treated cell are chromosomes that are misaligned at metaphase. (B) Lower magnification image (40 \times). Scale bars: 15 μ m.

characterized by chromosomes that fail to align properly on the metaphase plate. Evidence for chromosome alignment defects and chromosome segregation defects were found in prometaphase, metaphase, anaphase, telophase and early G1 cells (supplementary material Fig. S1). Additionally, we observed widened metaphase plates (defined as having a metaphase plate-width greater than 0.4 times the length of the metaphase plate) and an accumulation of mitotic cells. Overall, we found two subclasses of defective cells: cells with a well-defined and narrow metaphase plate containing several misaligned chromosomes, and cells with a loosely arranged metaphase plate and, generally, a larger number of misaligned

chromosomes (supplementary material Fig. S2). These subclasses typically comprise 65% and 35%, respectively, of the mitotic population in AdOx-treated groups. These groups will be referred to simply as 'well-defined' and 'poorly defined'. Visual scoring of over 300 mitotic cells per experiment showed a 6.7-fold increase in the number of mitotic cells with these defects upon exposure to AdOx. No obvious changes in interphase cells were observed during this brief treatment, indicating that the entry into mitosis was particularly sensitive to inhibition of protein methylation.

AdOx treatment decreases the apparent abundance of H3K9me3 and H4K20me3

IIF and immunoblotting of several methylated histones (H3K9me1, H3K9me2, H3K9me3, H3K4me3, H4K20me1 and H4K20me3) were performed to establish which methylation moieties are affected. These experiments were performed on both asynchronous and mitotic cell populations to determine whether there are any decreases in methylation of the tested sites and, if so, at what points in the cell cycle they occur. Interestingly, after 2 hours of exposure to AdOx, none of the methylated species tested were seen to decrease in an asynchronous cell population. It was only when mitotic populations were tested that a decrease of any methylated species became apparent (Fig. 2). Several methylated isoforms of histones, including H3K9me1, H3K9me2 and H3K4me3, remained stable in both asynchronous and mitotic populations (images of H3K4me3 are shown in supplementary material Fig. S3). By contrast, H3K9me3 and H4K20me3 showed a marked decrease in intensity in the mitotic portion. As measured by IIF, H3K9me3 intensity in treated cells was 0.64 ± 0.03 times the intensity of control cells and, in the case of H4K20me3, 0.62 ± 0.08 times the intensity of control cells. Antibody specificity was verified by using a peptide competition assay (supplementary material Fig. S4). The decrease measured by immunoblotting was similar (0.61 ± 0.05 times the intensity of control cells for H3K9me3 and 0.54 ± 0.04 for H4K20me3). A less prominent, but still quantifiable, decrease in methylation intensity was also found for H4K20me1: 0.80 ± 0.04 times the intensity of control cells when measured by IIF. The decrease of H4K20me1 is important to note as a positive control for our study because this modification is known to increase in late G2 (Pesavento et al., 2008; Rice et al., 2002; Xiao et al., 2005). Of the modified histone groups measured, it would seem that the mitotic defects resulting from loss of methylation are most closely correlated with H3K9me3 and H4K20me3 (Table 1). Our results show that specific methylated histones undergoing methylation during G2

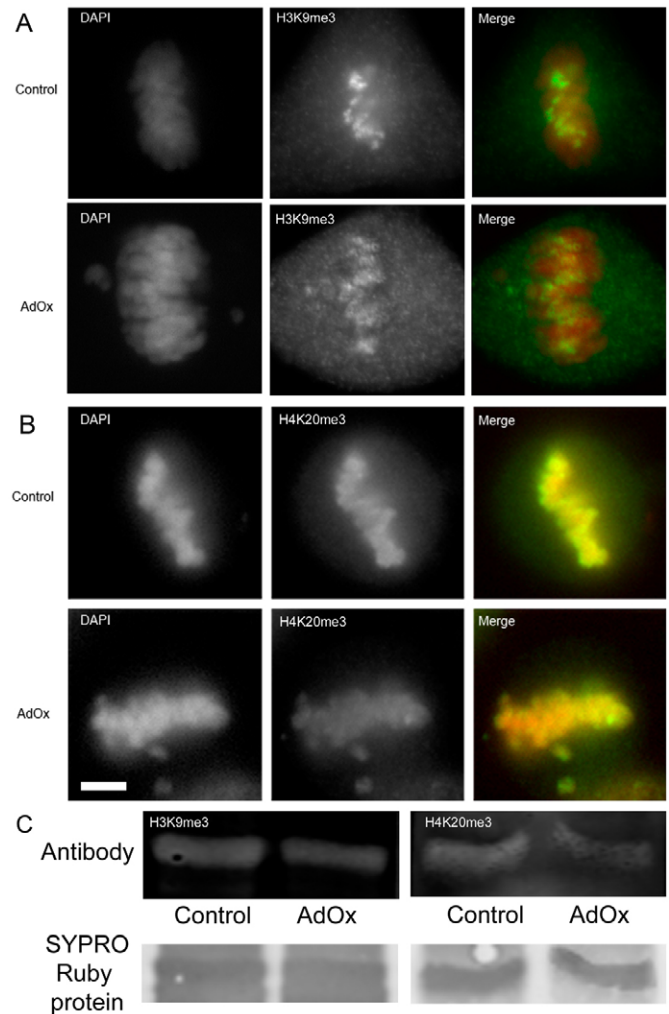


Fig. 2. Altered histone methylation levels in AdOx-treated HeLa cells. Asynchronous HeLa cells were grown overnight, paraformaldehyde-fixed and stained with DAPI and anti-H3K9me3 (A) or DAPI and anti-H4K20me3 (B). (A,B) Representative metaphase cells of both control cells (top row in both A and B) and cells treated with AdOx for 2 hours (bottom row in both A and B). The right-hand column of both A and B is a merged image of both wavelengths; the methylation antibodies are shown in green and DAPI is shown in red. (C) Western blots of mitotic cells treated with the same antibodies as in A and B. SYPRO Ruby protein blot stain confirms protein loading. Scale bar: 7 μ m.

Table 1. Histone modifications affected by methylation inhibition

Histone modification studied	Intensity difference in unsynchronized cells	Intensity difference in mitotic cells	Intensity drop in AdOx-treated mitotic cells*	
			IIF	WB
H3K9me1	No	No	–	–
H3K9me2	No	No	–	–
H3K9me3	No	Yes	0.64 ± 0.03	0.61 ± 0.05
H4K20me1	No	Yes	0.80 ± 0.04	–
H4K20me3	No	Yes	0.62 ± 0.08	0.54 ± 0.04
H3K4me3	No	No	–	–

Integrated intensities of several modified histone species were measured and compared between a control group and an AdOx-treated group. Differences in intensity were noted and quantified when present. This experiment was performed on both unsynchronized cell populations and mitotic cell populations. Mitotic cells were isolated by mitotic shakeoff. Differences in intensity were determined by quantitative measurements of both indirect immunofluorescence (IIF) images and western blotting (WB) of nuclear extracts.

*AdOx intensity divided by control intensity.

correspond to methylated histones that are enriched in pericentric heterochromatin (Peters et al., 2003; Schotta et al., 2004; Sullivan and Karpén, 2004).

Loss of H3K9me3 does not account for the full severity of the defect seen after inhibiting global methylation

H3K9me3 and H4K20me3 are species that we found to be the most affected by an inhibition of methylation, however, this does not address the issue of whether these moieties account for the full severity of the defect in chromosome alignment seen with AdOx treatment. In order to determine the extent of the influence of these histone modifications in chromosome segregation, we compared the severity of the defect in two mouse epithelial fibroblast cell lines: *SUV39h1/h2^{-/-}* and the parental cell line. *SUV39h1/h2^{-/-}* cells lack the methyltransferases responsible for the trimethylation of H3K9 and, as a consequence, lack any H3K9me3 in pericentric heterochromatin (Peters et al., 2001). H4K20me3 is also decreased globally and lost from heterochromatin in these null cells (Siddiqui et al., 2007). Wild-type and *SUV39h1/h2^{-/-}* mouse embryonic

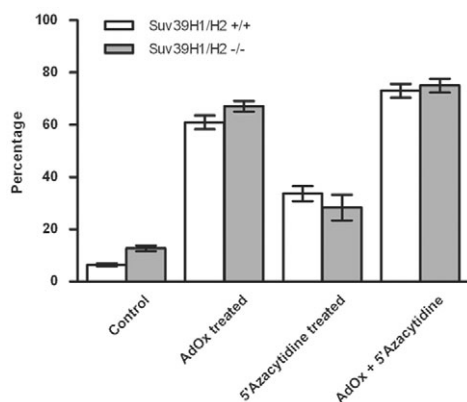


Fig. 3. H3K9me3, H4K20me3 and DNA methylation do not account for the full severity of the mitotic defect seen with AdOx treatment. The severities of metaphase defects were compared between various treatment groups of both wild-type (*SUV39h1/h2^{+/+}*) and *SUV39h1/h2^{-/-}* mouse embryonic fibroblast cell lines. Cells were synchronized with a double thymidine block and released. All treatment groups were fixed 8 hours after double thymidine release to allow for mitotic enrichment. The treatment groups were scored for metaphase cells containing misaligned chromosomes and the result expressed as the percentage of total metaphase cells that were scored as misaligned. Percentages and standard deviations were calculated from the averages of three separate trials, each with a minimum of 50 cells (data shown in Table 2).

fibroblast cell lines were synchronized using a double thymidine block and released. 5'-Azacytidine was added immediately following release from the double thymidine block in the applicable treatment groups and AdOx was added 6 hours after the double thymidine block in the applicable treatment groups. All treatment groups were fixed at 8 hours after double thymidine block to allow enrichment of mitotic cells (supplementary material Fig. S5). The percentage of cells containing lagging chromosomes and the standard deviations (Fig. 3) were calculated from the averages of three separate trials (data shown in Table 2).

From these data we note several findings. The ~twofold increase in the number of defective metaphase cells between control *SUV39h1/h2^{-/-}* cells and the control parental cell line confirms that H3K9me3 plays a role in mitosis. The increase in the proportion of defective cells seen with AdOx treatment in H3K9me3-deficient cells, however, provides evidence that additional methylated species play a role. This is supported by the additional finding that siRNA knockdown of SUV420h1 and SUV420h2 in *SUV39h1/h2^{-/-}* cells shows no significant increase in the proportion of mitotic cells that contain mis-segregated chromosomes (supplementary material Fig. S6). The same knockdown of SUV420h1 and SUV420h2 in the parental cell line, however, leads to an increase in chromosomal alignment defects such that the wild-type and knockout cells, without AdOx, show the same level of defect. This suggests that H4K20me3 in pericentric heterochromatin plays an important role in mitotic chromosome alignment because *SUV39h1/h2^{-/-}* cells also lack pericentric H4K20me3, although they still contain H4K20me3 along the chromosome arms (Schotta et al., 2004). The fact that the knockout cells show no apparent increase in chromosomal alignment defects when global H4K20me3 is lost, whereas the parental cell line does, gives support to the importance of pericentric H4K20me3. Several papers have shown, however, that knockout of SUV420h1 and SUV420h2 leads to the near complete loss of both H4K20me3 and H4K20me2 (Sakaguchi et al., 2008; Schotta et al., 2008). It is possible that the loss of dimethylation of histone H4 at lysine 20 is responsible for the observed changes or contributes to the phenotype. However, *SUV39h1/h2^{-/-}* cells lack proper localization of H4K20me3 but reportedly retain H4K20me2 (Schotta et al., 2004). Because H4K20me2 is retained in *SUV39h1/h2^{-/-}* cells, the similar proportion of mitotic defects observed with knockdown of SUV420h1 and SUV420h2 in wild-type cells and in the *SUV39h1/h2^{-/-}* cells means that the loss of H4K20me3 is the only known change in methylation that is common to both cell types.

Table 2. Mitotic cells containing lagging chromosomes after drug treatment

Drug treatment	Cell type	Average number of mitotic cells with lagging chromosomes	Average total number of mitotic cells	Percentage of cells with lagging chromosome
Control	WT	3	53	6
	KO	7	53	13
AdOx	WT	34	56	61
	KO	38	57	67
5'-Azacytidine	WT	18	52	34
	KO	16	56	29
AdOx + 5'-azacytidine	WT	36	49	73
	KO	39	52	75

The severities of metaphase defects were compared between various treatment groups of both wild-type (WT; *SUV39h1/h2^{+/+}*) and knockout (KO; *SUV39h1/h2^{-/-}*) mouse embryonic fibroblast cell lines. Groups were treated with either AdOx or AdOx plus 5'-azacytidine and scored for mitotic cells containing misaligned (lagging) chromosomes. Percentage of cells with misaligned chromosomes is given as a percentage of total mitotic cells. Data are shown graphically in Fig. 3.

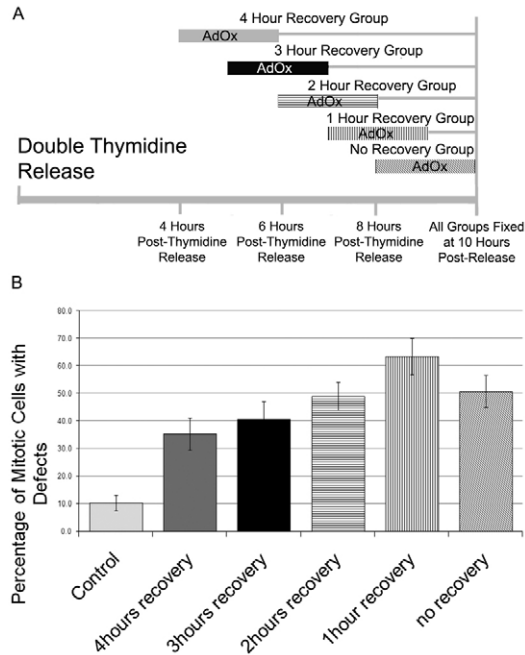


Fig. 4. Pulsed inhibition of methylation reveals an important window of ongoing methylation occurring 1-3 hours prior to mitosis. A double thymidine block was used to synchronize cells in S-phase. At varying times after release from the S-phase block, treatment groups had 250 μ M AdOx added for 2 hours and then the media was replaced with fresh media without drug. All groups were allowed to progress for 10 hours after initial thymidine release and then fixed. A minimum of 50 cells were then scored to determine what percentage of mitotic cells showed the described defects. This experiment was repeated three times. (A) Graphical representation of the treatment window and experimental protocol. (B) Percentage of mitotic cells scored that showed defects in each treatment group. Error bars indicate standard deviations.

We also found that a decrease in DNA methylation with 5'-azacytidine treatment led to an increased defective portion of metaphase cells in both cell lines (Fig. 3, Table 2); however, there was an additive effect when cells were treated with both AdOx and 5'-azacytidine concomitantly. This leads us to believe that the mitotic alignment defects seen with AdOx treatment is affected by more than the loss of H3K9me3, H4K20me3 and DNA methylation. All comparisons made were statistically significant ($P < 0.05$, Student's *t*-test).

Methylation is crucial for chromosome segregation 1-3 hours prior to mitosis

We were interested in further defining the timing of the methylation event(s) crucial for proper progression through mitosis. Cells were synchronized in early S phase with a double thymidine block and then released. Upon release, cells proceed through S phase, G2 and mitosis with synchronized timing. Control cells were found to contain the largest proportion of mitotic cells 9-11 hours post-release. Experimental groups of cells were pulse-treated with AdOx for 2-hour windows, washed with phosphate buffered saline (PBS) and fresh media added. The AdOx pulse treatment began at 4, 5, 6, 7 and 8 hours after release of the S-phase block. All groups were fixed at 10 hours, corresponding to the time period of the mitotic peak of the control cell population (Fig. 4A). Although all time points showed a significant increase in the proportion of defective cells observed in mitosis, the largest increase in defective cells

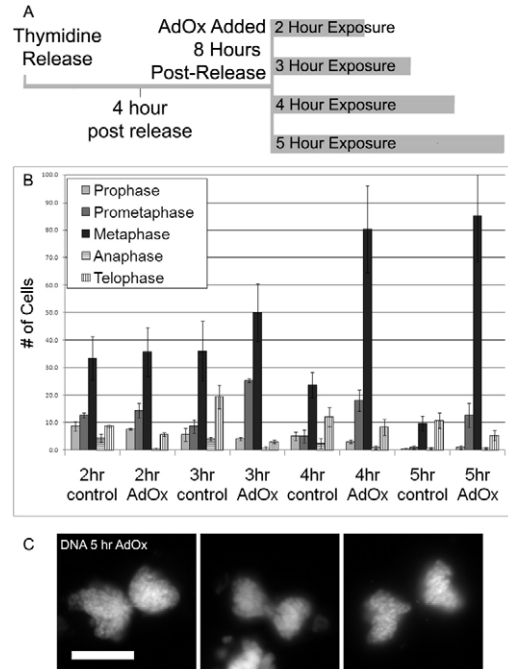


Fig. 5. Metaphase-anaphase checkpoint is active but checkpoint failure eventually occurs in some cells. A double thymidine block was used to synchronize HeLa cells at S phase. Cells were released from thymidine block and allowed to progress for 8 hours, at which point 250 μ M AdOx was added. Cells were then fixed at varying time points and counted in order to determine the number of cells in each phase of mitosis. (A) Graphical presentation of the experimental design. Time of the experiment progresses from left to right. At 8 hours, the cells were separated into four treatment groups in order to vary the length of treatment. (B) Number of cells in each phase of mitosis for each treatment group out of a total of 350 cells counted. Error bars indicate standard deviations. (C) An image of DAPI-stained chromatin in telophase-early G1 cells typical of cells counted in the telophase of the 5-hour AdOx group. Scale bar: 25 μ m.

occurred when AdOx was administered 3 hours prior to fixation (Fig. 4B). This crucial period corresponds to late G2 and overlaps with the pulse of H3K9 trimethylation described in our earlier manuscript (McManus et al., 2006).

Mitotic checkpoint activation with AdOx treatment

We next determined whether these methylation events affected the mitotic checkpoint, a pathway that inhibits the progression of a metaphase cell into anaphase until all kinetochores are correctly and stably connected by microtubules to the mitotic spindles (Chan et al., 2005). To test this, cells were synchronized with a double thymidine block and released for 8 hours into fresh medium. At 8 hours after the release from the S-phase block, AdOx was added with increasing length of treatment times ranging from 2 to 5 hours (Fig. 5A). Cells were then fixed and mitotic cells counted and compared to control groups. As noted earlier, mitotic enrichment was highest between 9 and 11 hours after the release of the S-phase block in control cells. By contrast, the AdOx-treated cells show continued accumulation of metaphase cells from the 10-hour time point (2 hours of treatment) to the 13-hour time point (5 hours of treatment). Moreover, the proportion of anaphase and telophase cells decreased as compared with untreated cells (Fig. 5B). Both findings demonstrate an activated and functional mitotic checkpoint. It is

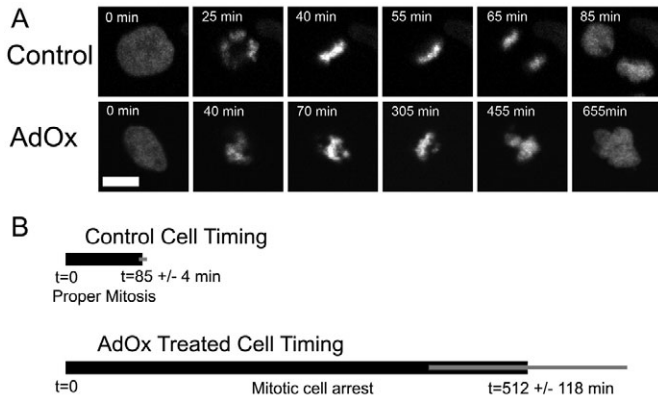


Fig. 6. Time-lapse microscopy of stably transfected histone H2B-GFP HeLa cells. (A) Representative digital images of two cells undergoing mitosis are shown to compare an untreated H2B-GFP cell (top) with an AdOx-treated cell (bottom). AdOx was added 3 hours prior to imaging. The first image in each series ($T=0$) was taken 25 minutes before the first indication of mitosis (prometaphase staining pattern). The proceeding images are then matched between treated and untreated according to the apparent stage in the cell cycle. The final image in each series was taken 10 minutes after DNA was full decondensed (as determined by the absence of significant further nuclei expansion). The time of each image relative to the first in both series is shown. Images were collected on a spinning disk confocal microscope at $20\times$ and at 5-minute intervals to minimize phototoxicity. Scale bar: $25\ \mu\text{m}$. (B) Mean duration of mitosis in both the control (85 ± 4 minutes, $n=5$) and the AdOx-treated (512 ± 118 minutes, $n=5$) groups diagrammatically represents the extent of cell-cycle arrest. Error bars represent s.e.m. The mean of AdOx-treated minus control groups equals 427 minutes, $P<0.01$ (Student's *t*-test).

important to note that some telophase cells still appear with AdOx treatment, indicating either that this subset of cells progress through mitosis with proper chromosome alignment or that the checkpoint eventually fails. To distinguish between these two possibilities, we examined telophase cells and found that they commonly displayed chromosome bridges (Fig. 5C), a structure consistent with an eventual failure of the mitotic checkpoint.

To extend these results, we performed time-lapse microscopy on HeLa cells expressing histone H2B-GFP (histone H2B fused to green fluorescent protein). We found that mitotic cells treated with AdOx spent a considerable amount of time progressing through mitosis, due to the activation of the mitotic checkpoint (Fig. 6). A subset of chromosomes tended to become trapped at the spindle poles and this resulted in a failure to properly align chromosomes at metaphase. Interestingly, these chromosomes do not move from these positions, suggesting that they might fail to associate with microtubules. After a prolonged period without alignment of the chromosomes, the checkpoint eventually fails and the cells progress to the next interphase. The resulting post-mitotic cells are larger than normal, have irregular nuclear boundaries and are tetraploid. These findings show that although the mitotic checkpoint can fail after extended arrest, it is activated and, therefore, is largely unaffected by the loss of late G2 methylation events

Kinetochores are affected by loss of methylation

These results described above suggest that inhibition of G2 methylation caused defects in the centromere, kinetochore and/or microtubule structure and function. Consequently, we examined the assembly of microtubules and centromere and kinetochore proteins to determine whether or not the composition of either the centromere

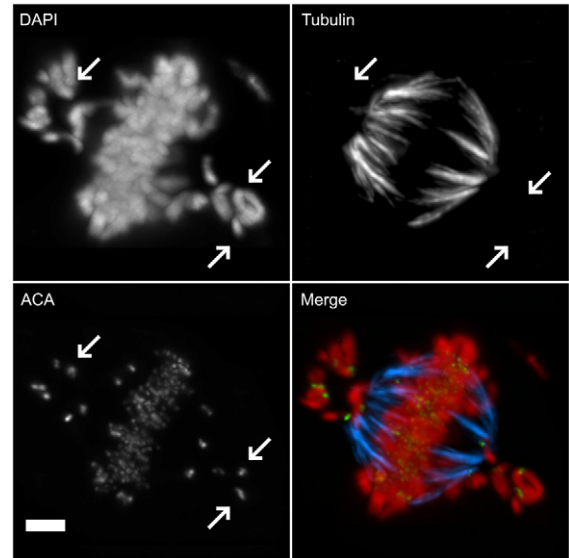


Fig. 7. CENH3, CENP-B and CENP-C localize properly in AdOx-treated cells whereas microtubules fail to stably attach to kinetochores. Asynchronous HeLa cells were grown overnight on coverslips, paraformaldehyde-fixed and stained with DAPI, anti-ACA and anti-tubulin. Prior to fixation, cells underwent cold destabilization of unattached microtubules so that only microtubules stably attached to kinetochores remained intact. Cells were then visualized and a representative cell is shown. All four images depict the same AdOx-treated cell with different combinations of antibodies. Arrows show misaligned, unattached centromeres. Scale bar: $5\ \mu\text{m}$.

or the kinetochore was altered. The most obvious candidate for study is tubulin, which can indicate whether defective microtubules play a role in the observed disorganized metaphase plate. Microtubules that are not stably bound to kinetochores can be dissociated by adding ice-cold media (Brinkley and Cartwright, 1975) and so this technique (termed 'cold destabilization') was used to observe only the kinetochore-bound subset of microtubules. In this experiment it was clear that microtubules failed to stably associate with the misaligned chromosomes (as denoted by the arrows in Fig. 7). This defect appears to be restricted to the misaligned kinetochores because the microtubules remain stable when associated with the chromosomes within the metaphase plate.

CENH3 is another centromeric protein that is crucial for proper mitotic division. CENH3 is a H3 homolog that replaces H3 in nucleosomes within the centromere (Palmer et al., 1991; Warburton et al., 1997). Anti-centromeric antigen (ACA) stains the centromeres of cells by binding to CENH3, CENP-B and CENP-C. We found no difference in ACA staining patterns following methylation inhibition. Misaligned chromosomes and aligned chromosomes both displayed proper ACA staining (Fig. 7).

The literature describes many mitotic segregation defects that are similar to those noted here and implicate certain kinetochore proteins in the defect (Bomont et al., 2005; Chan et al., 2000; Chan et al., 1999; Feng et al., 2006; Holt et al., 2005; Kallio et al., 2002; Liao et al., 1995; Maia et al., 2007; Mao et al., 2005; Morrow et al., 2005; Musio et al., 2004; Rattner et al., 1993; Tanudji et al., 2004; Yao et al., 2000; Yen et al., 1992). Kinetochore proteins that have been implicated include CENP-F, Aurora-B, CENP-E, BUBR1 and ZW10. We have determined the effect of AdOx treatment on the localization of kinetochore proteins to determine whether their

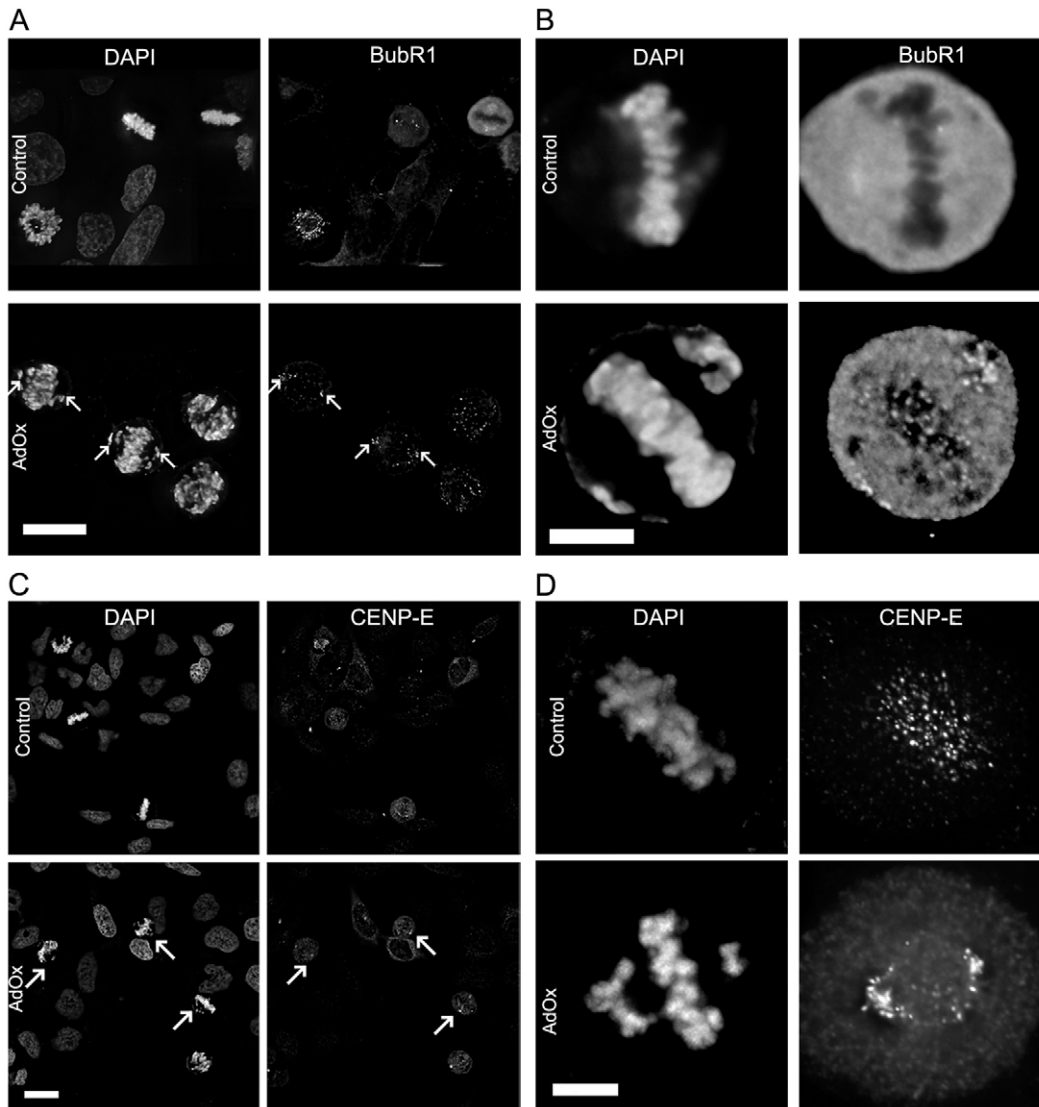


Fig. 8. Kinetochores proteins accumulate on chromosomes that are misaligned following AdOx treatment. HeLa cells were fixed with paraformaldehyde after growing overnight. (A,B) Cells were transfected with BUBR1-GFP and stained with DAPI. (C,D) Coverslips of cells were stained with anti-CENP-E antibody and DAPI. Control cells are compared with AdOx-treated cells. Arrows in low-resolution pictures (A,C) show the misaligned chromosomes. (B,D) Higher magnification images. Scale bars: 15 μ m (A,C); 5 μ m (B,D).

improper localization plays a role. Several proteins that were studied showed no obvious change in abundance or in localization. Among these were CENP-F, a microtubule-binding protein that is required for kinetochore attachment and the mitotic checkpoint (Bomont et al., 2005; Feng et al., 2006; Holt et al., 2005; Liao et al., 1995; Rattner et al., 1993), and Aurora B (also known as AIM-1), a mitotic checkpoint protein kinase (Kallio et al., 2002; Morrow et al., 2005) (supplementary material Figs S7 and S8).

Several proteins needed for proper chromosome segregation did show altered localization patterns when exposed to AdOx for 2 hours: CENP-E, BUBR1 and ZW10 (Chan et al., 2000; Chan et al., 1999; Maia et al., 2007; Mao et al., 2005; Musio et al., 2004; Tanudji et al., 2004; Yao et al., 2000; Yen et al., 1992). These three proteins showed similar results. In control cells, all three proteins were found localized to the kinetochores in prophase and prometaphase. Upon stable binding of microtubules, CENP-E, ZW10 and BUBR1 began to depart from the kinetochores and the staining pattern became cytoplasmic. At late metaphase, immediately prior to the beginning of anaphase, all three of these proteins were completely depleted from the metaphase plate. Their depletion is believed to occur once microtubules have stably bound

to kinetochores and is, once completed, indicative of the resolution of the mitotic checkpoint (Musacchio and Salmon, 2007). In AdOx-treated metaphase cells with unaligned chromosomes, these three proteins were found to be depleted from the metaphase plate. This correlates with microtubule attachment. However, the misaligned chromosomes were each found to have an increased kinetochore localization of all three proteins as compared with control cell chromosomes (CENP-E and BUBR1 are shown in Fig. 8). This is consistent with a mechanism whereby cells can relocate CENP-E, ZW10 and BUBR1 to misaligned chromosomes to increase microtubule stabilization or chromosome alignment, a mechanism already described for some kinetochore proteins (Gorbsky and Ricketts, 1993; Skoufias et al., 2001; Waters et al., 1998).

Interkinetochore distance in AdOx-treated cells indicates changes in tension or structural abnormalities

Both H3K9 and H4K20 trimethylation play major roles in heterochromatin formation and chromatin compaction and are found in pericentric heterochromatin (Melcher et al., 2000; Peters et al., 2003; Schotta et al., 2004; Sullivan and Karpen, 2004). These moieties are also found to decrease with AdOx treatment. We wished

to determine whether the loss of methylation caused by AdOx treatment affected pericentric heterochromatin structure and whether a relaxed centromere could explain the widened metaphase plate. To address this possibility, HeLa cells were stained with anti-ACA to identify the kinetochores. Three-dimensional confocal images were obtained by deconvolution of a through-focus z-series and analyzed. In high-resolution deconvolved images, it was possible to resolve both kinetochores found on each chromosome. The interkinetochore distance has been used as an indication of the amount of tension present on each individual chromosome (Waters et al., 1996).

Interkinetochore distance was measured in four experimental groups: control cells and AdOx-treated cells with and without cold destabilization of microtubules (Fig. 9A, Table 3). A representative image of those used to obtain measurements is shown in Fig. 9B and at higher magnification in Fig. 9C. In HeLa cells without cold destabilization, interkinetochore distance decreased upon exposure to AdOx in both the well- and poorly defined subsets, illustrating a decrease in tension. Interestingly, the interkinetochore distance

decreases in control cells with cold destabilization but does not in AdOx-treated cells. All comparisons noted are statistically significant ($P < 0.05$, Student's *t*-test). As expected, misaligned chromosomes, regardless of cold destabilization, have a significantly smaller interkinetochore distance that is comparable to the distance of unattached kinetochores, as shown by the nocodazole-treated group. These findings confirm that the misaligned chromosomes do not have any microtubule attachments that are able to generate tension, and also demonstrate that aligned chromosomes might have structural defects that interfere with the transmission of tension through the centromere.

Transmission electron microscopy shows structural defects in AdOx-treated mitotic cells

The observed loss of tension at the metaphase plate in cells where methylation was inhibited implies that the centromeric structure might be affected. We therefore carried out a structural study with transmission electron microscopy (TEM) to determine whether or not there were any changes in the structure of the chromosomes and/or kinetochores. Figs 10A and 10B shows examples of treated mitotic cells and control cells. Unlike the control cell, where the centromere and kinetochore are well defined, the drug-treated cells show several differences: centromeric chromatin was slightly expanded and the relationship between centromere and kinetochore was disrupted. Generally, there was a loosening of the kinetochore and centromere structure. It was also noted that some kinetochores of chromosomes within the metaphase plate in the poorly defined subset were also found with few or no microtubules attached (Fig. 10B). Counts of kinetochores within control and treated cells show that the percentage of aberrant kinetochores increases from 13 to 59% (Fig. 10C) when treated with AdOx. Findings from the TEM experiments confirm that there are major structural abnormalities when methylation is inhibited in late G2.

Discussion

The defect in mitotic alignment caused by inhibition of methylation reported here is similar to a defect described in an earlier paper from this laboratory (McManus et al., 2006) wherein a stable mouse cell line deficient in SUV39h1 and SUV39h2 was found to have mitotic defects. The timing of AdOx treatment that resulted in the most severe phenotype coincided with the timing of the mitotic increase in lysine 9 trimethylation that we described previously (McManus et al., 2006). In this study, although we have provided further evidence for this dynamic methylation of lysine 9 during mitosis, our results imply that there are additional methylation events that occur during G2 that are important in the regulation of mitotic processes. The mitotic defect seen with global loss of active methylation is more severe than that seen in *SUV39h1/h2*^{-/-} cells.

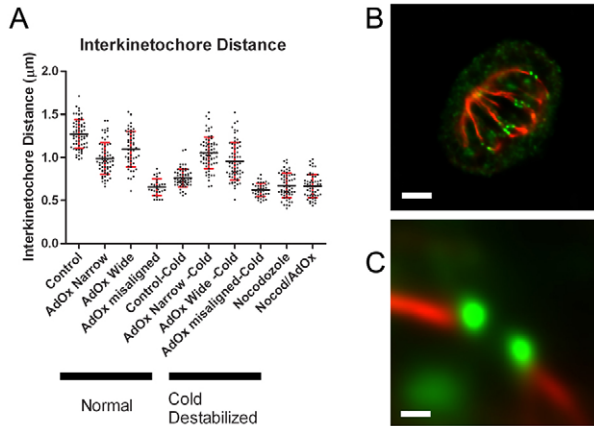


Fig. 9. Interkinetochore distance of four groups. Interkinetochore distance was measured and grouped according to experimental group and phenotype. The four experimental groups are control and AdOx-treated groups with and without cold destabilization of microtubules. The AdOx-treated groups were further subdivided according to phenotype: cells with a well-defined metaphase plate (narrow) and cells with a poorly defined metaphase plate (wide). Also measured were misaligned chromosomes and, as a positive control for unattached kinetochores, nocodazole-treated cells with and without AdOx. (A) Individual distances are marked on a dot plot with the mean shown. Red error bars are standard deviation. Data are given in Table 3. (B) Example image of a cell used for measurement. Microtubules are shown in red and ACA staining is shown in green. Scale bar: 4 µm. (C) Higher magnification of one kinetochore set. Scale bar: 0.4 µm.

Table 3. Interkinetochore distance in AdOx-treated cells

	Without cold destabilization				With cold destabilization				Nocodazole	Nocodazole with AdOx
	Control	AdOx			Control	AdOx				
Interkinetochore distance	Control	Narrow	Wide	Misaligned	Control	Narrow	Wide	Misaligned		
Mean	1.27	0.99	1.10	0.66	0.76	1.06	0.96	0.62	0.67	0.67
Standard deviation	0.17	0.18	0.21	0.10	0.10	0.18	0.22	0.08	0.14	0.13

Interkinetochore distance was measured in four experimental groups: control and AdOx-treated groups with and without cold destabilization of microtubules. The AdOx-treated groups were further subdivided according to phenotype: cells with a well-defined metaphase plate (narrow) and cells with a poorly defined metaphase plate (wide). Also measured were misaligned chromosomes and, as a measurement of unattached kinetochores, nocodazole-treated cells with and without AdOx. Data are shown graphically in Fig. 9.

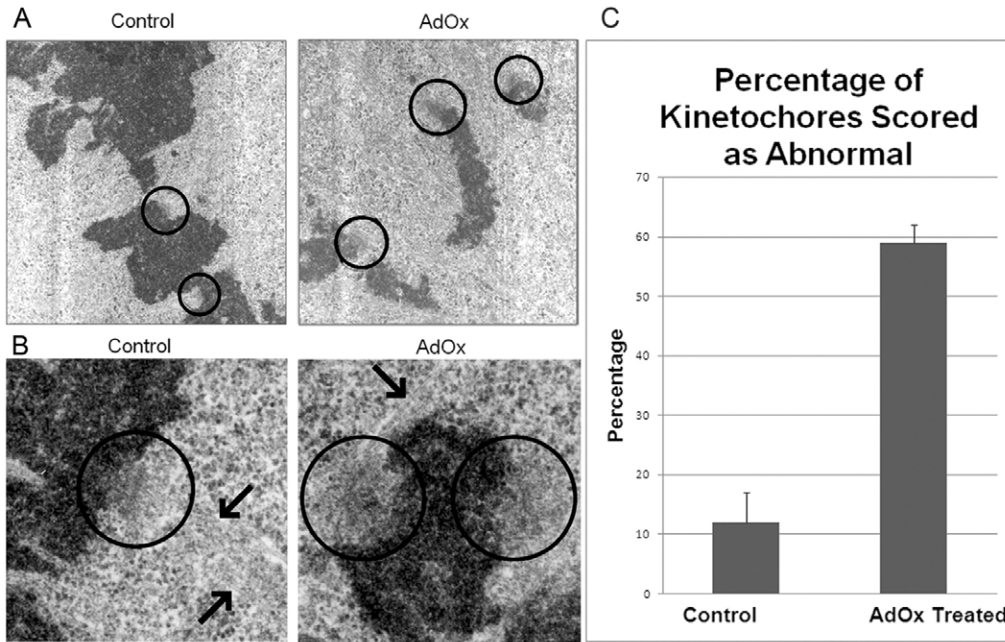


Fig. 10. Transmission electron microscopy (TEM) of mitotic HeLa cells reveals structural defects in the centromere and/or kinetochore following AdOx treatment. All images are of chromosomes that are aligned on the metaphase plate. (A) Kinetochores and underlying centromeric regions of chromatin are circled in black. (B) Higher magnification of kinetochores. Circles denote kinetochore and underlying centromere. Arrows highlight the microtubules. Note that there are no microtubules on the rightmost kinetochore in the AdOx treatment. (C) Counts of normal and abnormal kinetochores show a large increase in abnormal kinetochores with exposure to AdOx: 12±5% in control cells and 59±3% in AdOx-treated cells. A total of 20 cells were counted, with an average of 13 kinetochores counted per cell; over 250 kinetochores were counted in each experimental group. Error bars indicate standard deviations.

Our initial hypothesis that these methylation sites are crucial for kinetochore protein localization is not supported by our data. First, we have determined that the mitotic checkpoint is active and, second, we have shown that many kinetochore proteins localize properly and only show an over-accumulation on misaligned chromosomes once the metaphase plate begins to form. This leads us to believe that the kinetochore assembly pathway proceeds normally. The observed over-accumulation of a subset of kinetochore proteins can be explained by normal cell mechanisms. It is known that microtubule attachment causes the removal of several kinetochore proteins and that re-recruitment of two kinetochore proteins, BUBR1 and BUB1, has also been described earlier (Gorbsky and Ricketts, 1993; Skoufias et al., 2001; Waters et al., 1998). This indicates that the over-accumulation of kinetochore proteins observed upon loss of methylation might be a normal process that occurs in mitotic cells when chromosomes do not align properly.

If kinetochore formation seems not to be the major player, an additional role of methylation must be involved. H3K9me3 and H4K20me3 are enriched in pericentric heterochromatin and are required for the maintenance of heterochromatin integrity (Gonzalo et al., 2005; Schotta et al., 2004; Zinner et al., 2006). Thus, the finding that both of these modifications are drastically and preferentially affected by AdOx treatment suggests that disrupted heterochromatin formation and maintenance might cause the defective mitotic phenotype. This is supported by our TEM results and interkinetochore distance measurements, which show that AdOx treatment affects pericentric heterochromatin compaction and interkinetochore tension. Late G2 methylation might play a role in facilitating the further compaction of pericentric heterochromatin or in enhancing its stability in order to provide the rigidity required to transmit the tension applied by attached microtubules and/or to sense and stabilize these attachments. It should be noted that Pesavento and colleagues showed no change in H4K20me3 in mitosis (Pesavento et al., 2008); however, these findings were based on whole cell populations and were not able to distinguish any sub-phases of mitosis. The cell populations used to describe mitosis in that study were comprised of either a G2-M mix or a M-G1 mix

and therefore the temporal resolution required to distinguish metaphase, the point of maximum H4K20me3 intensity, from any other portion of cells was lacking. The IIF approach used here allowed us to detect changes in H4K20me3 measurements on an exclusively metaphase population.

Our results are consistent with a mechanism in which the loss of H3K9me3 and H4K20me3 from pericentric heterochromatin diminishes its structural integrity and leads to the mitotic defects we have described. Models of the chromatin structure in centromeres hold that CENH3 chromatin collects on one face of the chromatid, situated away from the sister chromatid, whereas pericentric heterochromatin is grouped together underlying the CENH3 chromatin (Cleveland et al., 2003; Dalal et al., 2007; Schueler and Sullivan, 2006; Sullivan and Karpen, 2004). The pulling force of microtubules is first transferred through the kinetochore, which is assembled on the CENH3 chromatin, and then through the underlying pericentric heterochromatin. Microtubule attachment is stabilized by tension between sister kinetochores and is believed to be destabilized by a lack of tension (Nicklas, 1997; Nicklas et al., 2001). The tension is believed to be sensed by various tension-monitoring kinetochore proteins at the inner centromere, potentially by altering the conformation of inner centromere proteins and so causing loss of activity (Baumann et al., 2007; Giemi et al., 2008). Once all chromosomes have uniform tension, the mitotic checkpoint is satisfied and, ultimately, cohesin, which can properly localize independent of H3K9me3 (Koch et al., 2008), is cleaved and anaphase begins (Chan et al., 2005).

Understanding this pathway enables us to understand how the loss of methylation fits into mitotic segregation. We can see that tension is required in this model for two reasons: for microtubule stabilization and to satisfy the mitotic checkpoint. Our findings fit this model due to the presence of misaligned chromosomes that fail to stably bind to microtubules and due to a robust mitotic checkpoint. In affected and visibly decondensed chromatin, the inability to transfer tension properly would lead to microtubule destabilization. Additionally, the inability to transfer tension through the pericentric heterochromatin to the inner centromere proteins would explain the

persistence of an activated mitotic checkpoint. We speculate that, although pericentric heterochromatin is present throughout the cell cycle, a large increase in methylation in late G2 and early mitosis is needed to stabilize or provide rigidity to the pericentric heterochromatin so that the centromeres and kinetochores have the rigid underlying structure needed for proper tension transmission to the inner centromere.

The profound consequences of this defect are seen in cells that have overridden the mitotic checkpoint and returned to interphase as tetraploid cells with irregular nuclear boundaries or as aneuploid cells with bridged chromosomes. This drastic increase in chromosomal instability (CIN) is important to note because CIN is known to be a precursor to cancer. It appears that increasing the amount of trimethylation of H3K9 and H4K20 during late G2 is crucial in providing structural integrity to the heterochromatin for effective mitosis and chromosomal stability. A burst of these epigenetic modifications might ensure that the alterations of heterochromatin structure that could have occurred over interphase (acetylation, demethylation, etc.) are countered by fresh heterochromatin compaction-initiating modifications prior to the crucial act of chromosome segregation during mitosis.

Materials and Methods

Cell culture

HeLa (human epithelial cervical carcinoma) cells were cultured in Dulbecco's modified Eagle's medium plus 10% fetal bovine serum in a 37°C incubator with 5% CO₂. Immortalized embryonic fibroblast cell lines from SUV39h1 and SUV39h2 double-null embryos were provided by Thomas Jenuwein (Peters et al., 2001).

Generation of HeLa cells stably expressing GFP constructs

Three stably transfected HeLa cell lines were used. One was stably transfected with H2B-GFP and another was stably transfected with ZW10-GFP. The final cell line was stably transfected with BUBR1-GFP.

Drug treatments

Live cells were treated with 250 mM AdOx (Sigma) for varying length of times. Cells were fixed, permeabilized and counterstained with 4',6-diamidino-2-phenylindole (DAPI), and phenotypic abnormalities were manually scored.

Cells treated with 5'-azacytidine were first synchronized at the G1-S boundary using a standard double thymidine block and released. Immediately following release, 5'-azacytidine was added to a final concentration of 3 μM.

Immunofluorescent labeling

Asynchronous cells were plated onto sterilized glass coverslips 1 day prior to immunostaining such that they were 50–80% confluent on the following day. Cells were fixed, permeabilized, immunofluorescently labeled and mounted as detailed elsewhere (McManus et al., 2006). The following primary antibodies were used at the dilutions indicated: anti-dMeK9 (1:200; Abcam), anti-tMeK9 (1:200; Abcam), anti-tMeLys4 (1:200; Abcam), anti-tMeK20 (1:200; Abcam) anti-centromeric antigen (1:1000; from G.K.T.C.), anti-CENP-E (1:1500; from G.K.T.C.), anti-CENP-F (1:1500; from G.K.T.C.), anti-tubulin (1:2000; from G.K.T.C.) and anti-phosphohistone H3 (Ser10) (1:400; Upstate Biotechnology, Lake Placid, NY). Appropriate secondary antibodies (e.g. mouse or rabbit) conjugated to fluorophores (e.g. Alexa Fluor 488 or Cy-3) were used for visualization of primary antibodies and were purchased from Molecular Probes (Eugene, OR) or Jackson ImmunoResearch Laboratories, and used at dilutions of 1:200.

Cold destabilization of microtubules

Cells were grown on coverslips as above. Prior to fixing, media was replaced with ice-cold media and incubated for 10 minutes on ice. Cells were then fixed by adding 2 ml of 3.5% paraformaldehyde in 100 mM PIPES at pH 6.8, 10 mM EGTA, 1 mM MgCl₂ and 0.2% Triton X-100. Cells were then washed with buffer A (10 mM Tris pH 7.5, 150 mM NaCl and 0.1% BSA) plus 0.2% Triton X-100 for 5 minutes, followed by a 5-minute wash in buffer A. Antibody staining proceeded as above.

Indirect immunofluorescence microscopy

Images were collected using MetaMorph (Universal Imaging) to control an Axiovert 200 M (Carl Zeiss MicroImaging) equipped and acquired with a 12-bit charge-coupled device camera (Sensicam; Cooke) or a 14-bit charge-coupled device camera (Cascade; Photometrics). GFP was excited using a Xenon or Argon lamp or a 488-nm laser line. For images acquired on fields of cells, either a 0.75 NA Fluor 20× objective

or a 1.3 NA Plan Fluor 40× objective (Carl Zeiss MicroImaging) was used. For higher magnification images, either a 1.4 NA Plan Apo 63× objective or a 1.4 NA Plan Apo 100× objective (Carl Zeiss MicroImaging) was used. Time-lapse experiments involving living cells were acquired at 37°C in standard Dulbecco's modified Eagle's medium with added fetal calf serum and a continuous CO₂ supply. Images were collected using Ultraview ERS (Perkin Elmer) coupled to an Axiovert 200 M (Carl Zeiss MicroImaging) equipped and acquired with the Ultraview ERS Rapid Confocal Imager.

Image processing and figure construction

Images were directly exported as 16-bit TIFF files and rescaled over an 8-bit data range. In most cases, the background fluorescence of the medium and the base signal from the detector were subtracted to better represent the dynamic range of the data content in the image. In some instances, three-dimensional image sets were imported into Imaris 5.7 (BitPlane) and three-dimensional image sets were generated. In this instance, the image was scaled to map the data over the range of the display, and the screen-capture function in Imaris 5.7 was used to capture the image used in the figures. Figures were prepared in Photoshop CS2 (Adobe) for Windows. In general, images were scaled to span the 8-bit data depth after subtraction of background in the process, and then pasted into a composite canvas that was either 8-bit grayscale or 24-bit RGB color. If necessary, images were interpolated to 300 dpi using Photoshop.

Immunoblot analysis

To confirm the availability and accessibility of all methylation epitopes and show their temporal regulation throughout the cell cycle, immunoblot analysis was conducted on protein extracts isolated from asynchronously growing cells and compared with extracts isolated from mitotic cells. HeLa cells were arrested at the G1-S phase boundary by standard double thymidine block, washed extensively with PBS, and permitted to progress for varying times. Asynchronous and subconfluent cells were harvested using 0.53 mM EDTA. Cells were pelleted by centrifugation at 500 g for 5 minutes at 4°C and resuspended in PBS. Following the final PBS wash, cells were lysed in nuclear isolation buffer (250 mM sucrose, 200 mM NaCl, 10 mM Tris-HCl at pH 8.0, 2 mM MgCl₂, 1 mM CaCl₂, 1% Triton X-100 and 1 mM phenylmethanesulfonyl fluoride). Nuclei were pelleted and resuspended in 0.4 N H₂SO₄ and placed on ice for 30 minutes. Nuclear debris was cleared by centrifugation at 25,000 g for 10 minutes. Supernatants were collected and added to 60 μl of 1 M Tris (pH 8.0) and 40 μl of 10 N NaOH.

The acid-extracted proteins from 2.0×10^5 asynchronously growing and mitotic-arrested cells were resolved on an 18% SDS-polyacrylamide gel. Protein loading was confirmed by SYPRO Ruby protein blot stain (Molecular Probes) and visualized on the Typhoon Imager 8600 (Amersham Biosciences). Proteins were transferred to 0.2 μm nitrocellulose membranes, blocked with 5% BSA in Tris-buffered saline (TBS) for one hour, and incubated with the appropriate antibody in 5% BSA in TBS plus 0.05% Tween, with shaking for one hour. Immunoblots were then incubated with IR800-conjugated secondary antibodies in the dark (1:12,000; Rockland Immunochemicals). Fluorescence imaging of the immunoblots was performed on the Odyssey Imaging System (Li-Cor Biosciences) as described by the manufacturer.

Electron microscopy

Cells were grown on 35-mm cell culture dishes and with or without the addition of AdOx as described above. The samples were fixed in 3% glutaraldehyde in Millonig's phosphate buffer for 1 hour. The samples were then washed in buffer and post-fixed in 2% OsO₄ for 20 minutes. The samples were then passed through a graded ethanol series and then infiltrated with Polybed 812 resin. Polymerization was performed at 60°C for 24 hours. Portions of the embedded cell monolayer containing cells of interest were selected by light microscopy and cut from the epon disc and mounted on epon blanks. Silver-gray sections were cut with a ultramicrotome (Leica) equipped with a Dumont (Hatfield PA) diamond knife and sections were stained with uranyl acetate and lead citrate and examined in a Hitachi H-7000 electron microscope.

Flow cytometry

Cells were grown on 10-cm cell culture dishes with and without the addition of AdOx as described above. The cells were then removed from the plate with the addition of trypsin for 5 minutes, spun down for 10 minutes at 500 g and resuspended in 0.5 ml PBS. The resuspended cells were then added to 70% ethanol for fixation and left at -20°C overnight. Cells were then collected by centrifugation, resuspended and rinsed in PBS and re-collected by centrifugation. Pelleted cells were then resuspended in 500 μl PBS containing a final concentration of 20 μg/ml propidium iodide and 200 μg/ml RNase A and left in the dark for 30 minutes at room temperature. DNA analysis was then performed using a Becton Dickinson FACsort flow cytometer with a 488 laser and BD CellQuest Pro Software (BD Biosciences).

Peptide competition assay

To confirm the specificity of antibodies used, we performed a peptide competition assay using peptides obtained from Abcam. Immunoblot analyses were performed as described above. The antibody incubation step was performed in tandem for three experimental groups per antibody tested. The first group was the antibody to be tested alone, the second group was the same antibody after incubation with peptides specific

to the antibody's target and the third group was the same antibody after incubation with a non-specific peptide. Analysis of the resulting immunoblots was performed as above. The peptides used were obtained from Abcam and were as follows: H3K9me3 ab1773, H3K9me1 ab1771, H4K20me3 ab17567 and H4K20me1 ab17043.

siRNA knockdown

The knockdown of SUV420h1 and SUV420h2 was performed using the Lipofectamine RNAiMAX kit (Invitrogen) according to the manufacturer's instructions on cells grown on coverslips in a six-well dish. siRNAs against both SUV420h1 and SUV420h2 were obtained from Qiagen (catalogue numbers SI00235914 and SI01438367, respectively). Cells were then fixed in 4% paraformaldehyde four days post-transfection. Indirect immunofluorescence microscopy was then performed on the coverslips as described above.

We would like to thank Jakub Famulski (University of Alberta, Edmonton, Canada) for the generous donation of several stably transfected cell lines and antibodies, Alan Underhill (University of Alberta, Edmonton, Canada) for supplying siRNA against SUV420h1, and Thomas Jenuwein (Max-Planck Institute of Immunobiology, Freiburg, Germany) for the donation of *SUV39h1/h2^{-/-}* and matched wild-type cell lines. This work was supported by operating grants from the Alberta Cancer Board and the Canadian Institutes of Health Research. M.J.H. is a senior scholar of the Alberta Heritage Foundation for Medical Research.

References

- Agger, K., Cloos, P. A., Christensen, J., Pasini, D., Rose, S., Rappsilber, J., Issaeva, I., Canaani, E., Salcini, A. E. and Helin, K. (2007). UTX and JMJD3 are histone H3K27 demethylases involved in HOX gene regulation and development. *Nature* **449**, 731-734.
- Annunziato, A. T., Eason, M. B. and Perry, C. A. (1995). Relationship between methylation and acetylation of arginine-rich histones in cycling and arrested HeLa cells. *Biochemistry* **34**, 2916-2924.
- Bannister, A. J., Zegerman, P., Partridge, J. F., Miska, E. A., Thomas, J. O., Allshire, R. C. and Kouzarides, T. (2001). Selective recognition of methylated lysine 9 on histone H3 by the HP1 chromo domain. *Nature* **410**, 120-124.
- Bartel, R. L. and Borchardt, R. T. (1984). Effects of adenosine dialdehyde on S-adenosylhomocysteine hydrolase and S-adenosylmethionine-dependent transmethylation in mouse L929 cells. *Mol. Pharmacol.* **25**, 418-424.
- Baumann, C., Korner, R., Hofmann, K. and Nigg, E. A. (2007). PICH, a centromere-associated SNF2 family ATPase, is regulated by Plk1 and required for the spindle checkpoint. *Cell* **128**, 101-114.
- Bomont, P., Maddox, P., Shah, J. V., Desai, A. B. and Cleveland, D. W. (2005). Unstable microtubule capture at kinetochores depleted of the centromere-associated protein CENP-F. *EMBO J.* **24**, 3927-3939.
- Borun, T. W., Pearson, D. and Paik, W. K. (1972). Studies of histone methylation during the HeLa S-3 cell cycle. *J. Biol. Chem.* **247**, 4288-4298.
- Brinkley, B. R. and Cartwright, J., Jr (1975). Cold-labile and cold-stable microtubules in the mitotic spindle of mammalian cells. *Ann. NY Acad. Sci.* **253**, 428-439.
- Chan, G. K., Jablonski, S. A., Sudakin, V., Hittle, J. C. and Yen, T. J. (1999). Human BUBR1 is a mitotic checkpoint kinase that monitors CENP-E functions at kinetochores and binds the cyclosome/APC. *J. Cell Biol.* **146**, 941-954.
- Chan, G. K., Jablonski, S. A., Starr, D. A., Goldberg, M. L. and Yen, T. J. (2000). Human Zw10 and ROD are mitotic checkpoint proteins that bind to kinetochores. *Nat. Cell Biol.* **2**, 944-947.
- Chan, G. K., Liu, S. T. and Yen, T. J. (2005). Kinetochores structure and function. *Trends Cell Biol.* **15**, 589-598.
- Cimini, D., Mattiuzzo, M., Torosantucci, L. and Degross, F. (2003). Histone hyperacetylation in mitosis prevents sister chromatid separation and produces chromosome segregation defects. *Mol. Biol. Cell* **14**, 3821-3833.
- Cleveland, D. W., Mao, Y. and Sullivan, K. F. (2003). Centromeres and kinetochores: from epigenetics to mitotic checkpoint signaling. *Cell* **112**, 407-421.
- Cloos, P. A., Christensen, J., Agger, K., Maiolica, A., Rappsilber, J., Antal, T., Hansen, K. H. and Helin, K. (2006). The putative oncogene GASC1 demethylates tri- and dimethylated lysine 9 on histone H3. *Nature* **442**, 307-311.
- Dalal, Y., Furuyama, T., Vermaak, D. and Henikoff, S. (2007). Structure, dynamics, and evolution of centromeric nucleosomes. *Proc. Natl. Acad. Sci. USA* **104**, 15974-15981.
- De Santa, F., Totaro, M. G., Prosperini, E., Notarbartolo, S., Testa, G. and Natoli, G. (2007). The histone H3 lysine-27 demethylase Jmjd3 links inflammation to inhibition of polycomb-mediated gene silencing. *Cell* **130**, 1083-1094.
- Feng, J., Huang, H. and Yen, T. J. (2006). CENP-F is a novel microtubule-binding protein that is essential for kinetochores attachments and affects the duration of the mitotic checkpoint delay. *Chromosoma* **115**, 320-329.
- Fischle, W., Tseng, B. S., Dormann, H. L., Ueberheide, B. M., Garcia, B. A., Shabanowitz, J., Hunt, D. F., Funabiki, H. and Allis, C. D. (2005). Regulation of HP1-chromatin binding by histone H3 methylation and phosphorylation. *Nature* **438**, 1116-1122.
- Fodor, B. D., Kubicek, S., Yonezawa, M., O'Sullivan, R. J., Sengupta, R., Perez-Burgos, L., Opravil, S., Mechtler, K., Schotta, G. and Jenuwein, T. (2006). Jmjd2b antagonizes H3K9 trimethylation at pericentric heterochromatin in mammalian cells. *Genes Dev.* **20**, 1557-1562.
- Gieni, R. S., Chan, G. K. and Hendzel, M. J. (2008). Epigenetics regulate centromere formation and kinetochore function. *J. Cell Biochem.* **104**, 2027-2039.
- Gonzalo, S., Garcia-Cao, M., Fraga, M. F., Schotta, G., Peters, A. H., Cotter, S. E., Eguia, R., Dean, D. C., Esteller, M., Jenuwein, T. et al. (2005). Role of the RB1 family in stabilizing histone methylation at constitutive heterochromatin. *Nat. Cell Biol.* **7**, 420-428.
- Gorbsky, G. J. and Ricketts, W. A. (1993). Differential expression of a phosphopeptide at the kinetochores of moving chromosomes. *J. Cell Biol.* **122**, 1311-1321.
- Grewal, S. I. and Jia, S. (2007). Heterochromatin revisited. *Nat. Rev. Genet.* **8**, 35-46.
- Holt, S. V., Vergnolle, M. A., Hussein, D., Wozniak, M. J., Allan, V. J. and Taylor, S. S. (2005). Silencing Cenp-F weakens centromeric cohesion, prevents chromosome alignment and activates the spindle checkpoint. *J. Cell Sci.* **118**, 4889-4900.
- Hong, S., Cho, Y. W., Yu, L. R., Yu, H., Veenstra, T. D. and Ge, K. (2007). Identification of JmjC domain-containing UTX and JMJD3 as histone H3 lysine 27 demethylases. *Proc. Natl. Acad. Sci. USA* **104**, 18439-18444.
- Kallio, M. J., McClelland, M. L., Stukenberg, P. T. and Gorbsky, G. J. (2002). Inhibition of aurora B kinase blocks chromosome segregation, overrides the spindle checkpoint, and perturbs microtubule dynamics in mitosis. *Curr. Biol.* **12**, 900-905.
- Keller, B. T. and Borchardt, R. T. (1987). Adenosine dialdehyde: a potent inhibitor of vaccinia virus multiplication in mouse L929 cells. *Mol. Pharmacol.* **31**, 485-492.
- Klose, R. J., Yamane, K., Bae, Y., Zhang, D., Erdjument-Bromage, H., Tempst, P., Wong, J. and Zhang, Y. (2006). The transcriptional repressor JHDM3A demethylates trimethyl histone H3 lysine 9 and lysine 36. *Nature* **442**, 312-316.
- Koch, B., Kueng, S., Ruckebauer, C., Wendt, K. S. and Peters, J. M. (2008). The SUV39h-HP1 histone methylation pathway is dispensable for enrichment and protection of cohesin at centromeres in mammalian cells. *Chromosoma* **117**, 199-210.
- Kubicek, S., Schotta, G., Lachner, M., Sengupta, R., Kohlmaier, A., Perez-Burgos, L., Linderson, Y., Martens, J. H., O'Sullivan, R. J., Fodor, B. D. et al. (2006). The role of histone modifications in epigenetic transitions during normal and perturbed development. *Ernst Schering Res. Found. Workshop*, 1-27.
- Lachner, M., O'Carroll, D., Rea, S., Mechtler, K. and Jenuwein, T. (2001). Methylation of histone H3 lysine 9 creates a binding site for HP1 proteins. *Nature* **410**, 116-120.
- Lechner, M. S., Schultz, D. C., Negorev, D., Maul, G. G. and Raucher, F. J., 3rd (2005). The mammalian heterochromatin protein 1 binds diverse nuclear proteins through a common motif that targets the chromoshadow domain. *Biochem. Biophys. Res. Commun.* **331**, 929-937.
- Liao, H., Winkfein, R. J., Mack, G., Rattner, J. B. and Yen, T. J. (1995). CENP-F is a protein of the nuclear matrix that assembles onto kinetochores at late G2 and is rapidly degraded after mitosis. *J. Cell Biol.* **130**, 507-518.
- Maia, A. F., Lopes, C. S. and Sunkel, C. E. (2007). BubR1 and CENP-E have antagonistic effects upon the stability of microtubule-kinetochore attachments in *Drosophila* S2 cell mitosis. *Cell Cycle* **6**, 1367-1378.
- Mao, Y., Desai, A. and Cleveland, D. W. (2005). Microtubule capture by CENP-E silences BubR1-dependent mitotic checkpoint signaling. *J. Cell Biol.* **170**, 873-880.
- McManus, K. J., Biron, V. L., Heit, R., Underhill, D. A. and Hendzel, M. J. (2006). Dynamic changes in histone H3 lysine 9 methylations: identification of a mitosis-specific function for dynamic methylation in chromosome congression and segregation. *J. Biol. Chem.* **281**, 8888-8897.
- Melcher, M., Schmid, M., Aagaard, L., Selenko, P., Laible, G. and Jenuwein, T. (2000). Structure-function analysis of SUV39H1 reveals a dominant role in heterochromatin organization, chromosome segregation, and mitotic progression. *Mol. Cell Biol.* **20**, 3728-3741.
- Morrow, C. J., Tighe, A., Johnson, V. L., Scott, M. I., Ditchfield, C. and Taylor, S. S. (2005). Bub1 and aurora B cooperate to maintain BubR1-mediated inhibition of APC/CCdc20. *J. Cell Sci.* **118**, 3639-3652.
- Musacchio, A. and Salmon, E. D. (2007). The spindle-assembly checkpoint in space and time. *Nat. Rev. Mol. Cell Biol.* **8**, 379-393.
- Musio, A., Mariani, T., Montagna, C., Zambroni, D., Ascoli, C., Ried, T. and Vezzoni, P. (2004). Recapitulation of the Roberts syndrome cellular phenotype by inhibition of INCENP, ZWINT-1 and ZW10 genes. *Gene* **331**, 33-40.
- Nakayama, J., Rice, J. C., Strahl, B. D., Allis, C. D. and Grewal, S. I. (2001). Role of histone H3 lysine 9 methylation in epigenetic control of heterochromatin assembly. *Science* **292**, 110-113.
- Nicklas, R. B. (1997). How cells get the right chromosomes. *Science* **275**, 632-637.
- Nicklas, R. B., Waters, J. C., Salmon, E. D. and Ward, S. C. (2001). Checkpoint signals in grasshopper meiosis are sensitive to microtubule attachment, but tension is still essential. *J. Cell Sci.* **114**, 4173-4183.
- Palmer, D. K., O'Day, K., Trong, H. L., Charbonneau, H. and Margolis, R. L. (1991). Purification of the centromere-specific protein CENP-A and demonstration that it is a distinctive histone. *Proc. Natl. Acad. Sci. USA* **88**, 3734-3738.
- Pesavento, J. J., Yang, H., Kelleher, N. L. and Mizzen, C. A. (2008). Certain and progressive methylation of histone H4 at lysine 20 during the cell cycle. *Mol. Cell Biol.* **28**, 468-486.
- Peters, A. H., O'Carroll, D., Scherthan, H., Mechtler, K., Sauer, S., Schofer, C., Weipoltshammer, K., Pagani, M., Lachner, M., Kohlmaier, A. et al. (2001). Loss of the Suv39h histone methyltransferases impairs mammalian heterochromatin and genome stability. *Cell* **107**, 323-337.
- Peters, A. H., Kubicek, S., Mechtler, K., O'Sullivan, R. J., Derijck, A. A., Perez-Burgos, L., Kohlmaier, A., Opravil, S., Tachibana, M., Shinkai, Y. et al. (2003). Partitioning and plasticity of repressive histone methylation states in mammalian chromatin. *Mol. Cell* **12**, 1577-1589.

- Rattner, J. B., Rao, A., Fritzler, M. J., Valencia, D. W. and Yen, T. J. (1993). CENP-F is a ca 400 kDa kinetochore protein that exhibits a cell-cycle dependent localization. *Cell Motil. Cytoskeleton* **26**, 214-226.
- Rea, S., Eisenhaber, F., O'Carroll, D., Strahl, B. D., Sun, Z. W., Schmid, M., Opravil, S., Mechtler, K., Ponting, C. P., Allis, C. D. et al. (2000). Regulation of chromatin structure by site-specific histone H3 methyltransferases. *Nature* **406**, 593-599.
- Rice, J. C., Nishioka, K., Sarma, K., Steward, R., Reinberg, D. and Allis, C. D. (2002). Mitotic-specific methylation of histone H4 Lys 20 follows increased PR-Set7 expression and its localization to mitotic chromosomes. *Genes Dev.* **16**, 2225-2230.
- Robbins, A. R., Jablonski, S. A., Yen, T. J., Yoda, K., Robey, R., Bates, S. E. and Sackett, D. L. (2005). Inhibitors of histone deacetylases alter kinetochore assembly by disrupting pericentromeric heterochromatin. *Cell Cycle* **4**, 717-726.
- Rougelle, C., Navarro, P. and Avner, P. (2003). Promoter-restricted H3 Lys 4 dimethylation is an epigenetic mark for monoallelic expression. *Hum. Mol. Genet.* **12**, 3343-3348.
- Sakaguchi, A., Karachentsev, D., Seth-Pasricha, M., Druzhinina, M. and Steward, R. (2008). Functional characterization of the Drosophila Hmt4-20/Suv4-20 histone methyltransferase. *Genetics* **179**, 317-322.
- Schoffa, G., Lachner, M., Sarma, K., Ebert, A., Sengupta, R., Reuter, G., Reinberg, D. and Jenuwein, T. (2004). A silencing pathway to induce H3-K9 and H4-K20 trimethylation at constitutive heterochromatin. *Genes Dev.* **18**, 1251-1262.
- Schoffa, G., Sengupta, R., Kubicek, S., Malin, S., Kauer, M., Callen, E., Celeste, A., Pagani, M., Opravil, S., De La Rosa-Velazquez, I. A. et al. (2008). A chromatin-wide transition to H4K20 monomethylation impairs genome integrity and programmed DNA rearrangements in the mouse. *Genes Dev.* **22**, 2048-2061.
- Schueler, M. G. and Sullivan, B. A. (2006). Structural and functional dynamics of human centromeric chromatin. *Annu. Rev. Genomics Hum. Genet.* **7**, 301-313.
- Shi, Y., Lan, F., Matson, C., Mulligan, P., Whetstone, J. R., Cole, P. A., Casero, R. A. and Shi, Y. (2004). Histone demethylation mediated by the nuclear amine oxidase homolog LSD1. *Cell* **119**, 941-953.
- Siddiqui, H., Fox, S. R., Gunawardena, R. W. and Knudsen, E. S. (2007). Loss of RB compromises specific heterochromatin modifications and modulates HP1 α dynamics. *J. Cell Physiol.* **211**, 131-137.
- Skoufias, D. A., Andreassen, P. R., Lacroix, F. B., Wilson, L. and Margolis, R. L. (2001). Mammalian mad2 and bub1/bubR1 recognize distinct spindle-attachment and kinetochore-tension checkpoints. *Proc. Natl. Acad. Sci. USA* **98**, 4492-4497.
- Smallwood, A., Esteve, P. O., Pradhan, S. and Carey, M. (2007). Functional cooperation between HP1 and DNMT1 mediates gene silencing. *Genes Dev.* **21**, 1169-1178.
- Smothers, J. F. and Henikoff, S. (2000). The HP1 chromo shadow domain binds a consensus peptide pentamer. *Curr. Biol.* **10**, 27-30.
- Stevens, F. E., Beamish, H., Warrener, R. and Gabrielli, B. (2008). Histone deacetylase inhibitors induce mitotic slippage. *Oncogene* **27**, 1345-1354.
- Sullivan, B. A. and Karpen, G. H. (2004). Centromeric chromatin exhibits a histone modification pattern that is distinct from both euchromatin and heterochromatin. *Nat. Struct. Mol. Biol.* **11**, 1076-1083.
- Tanudji, M., Shoemaker, J., L'Italien, L., Russell, L., Chin, G. and Schebye, X. M. (2004). Gene silencing of CENP-E by small interfering RNA in HeLa cells leads to missegregation of chromosomes after a mitotic delay. *Mol. Biol. Cell* **15**, 3771-3781.
- Tsukada, Y., Fang, J., Erdjument-Bromage, H., Warren, M. E., Borchers, C. H., Tempst, P. and Zhang, Y. (2006). Histone demethylation by a family of JmjC domain-containing proteins. *Nature* **439**, 811-816.
- Warburton, P. E., Cooke, C. A., Bourassa, S., Vafa, O., Sullivan, B. A., Stetten, G., Gimelli, G., Warburton, D., Tyler-Smith, C., Sullivan, K. F. et al. (1997). Immunolocalization of CENP-A suggests a distinct nucleosome structure at the inner kinetochore plate of active centromeres. *Curr. Biol.* **7**, 901-904.
- Waters, J. C., Skibbens, R. V. and Salmon, E. D. (1996). Oscillating mitotic newt lung cell kinetochores are, on average, under tension and rarely push. *J. Cell Sci.* **109**, 2823-2831.
- Waters, J. C., Chen, R. H., Murray, A. W. and Salmon, E. D. (1998). Localization of Mad2 to kinetochores depends on microtubule attachment, not tension. *J. Cell Biol.* **141**, 1181-1191.
- Xiang, Y., Zhu, Z., Han, G., Lin, H., Xu, L. and Chen, C. D. (2007). JMJD3 is a histone H3K27 demethylase. *Cell Res.* **17**, 850-857.
- Xiao, B., Jing, C., Kelly, G., Walker, P. A., Muskett, F. W., Frenkiel, T. A., Martin, S. R., Sarma, K., Reinberg, D., Gamblin, S. J. et al. (2005). Specificity and mechanism of the histone methyltransferase Pr-Set7. *Genes Dev.* **19**, 1444-1454.
- Xin, H., Yoon, H. G., Singh, P. B., Wong, J. and Qin, J. (2004). Components of a pathway maintaining histone modification and heterochromatin protein 1 binding at the pericentric heterochromatin in mammalian cells. *J. Biol. Chem.* **279**, 9539-9546.
- Yamada, T., Fischle, W., Sugiyama, T., Allis, C. D. and Grewal, S. I. (2005). The nucleation and maintenance of heterochromatin by a histone deacetylase in fission yeast. *Mol. Cell* **20**, 173-185.
- Yao, X., Abrieu, A., Zheng, Y., Sullivan, K. F. and Cleveland, D. W. (2000). CENP-E forms a link between attachment of spindle microtubules to kinetochores and the mitotic checkpoint. *Nat. Cell Biol.* **2**, 484-491.
- Yen, T. J., Li, G., Schaar, B. T., Szilak, I. and Cleveland, D. W. (1992). CENP-E is a putative kinetochore motor that accumulates just before mitosis. *Nature* **359**, 536-539.
- Zhang, C. L., McKinsey, T. A. and Olson, E. N. (2002). Association of class II histone deacetylases with heterochromatin protein 1, potential role for histone methylation in control of muscle differentiation. *Mol. Cell. Biol.* **22**, 7302-7312.
- Zinner, R., Albiez, H., Walter, J., Peters, A. H., Cremer, T. and Cremer, M. (2006). Histone lysine methylation patterns in human cell types are arranged in distinct three-dimensional nuclear zones. *Histochem. Cell Biol.* **125**, 3-19.